Polymer Testing 156 (2026) 109132

Contents lists available at ScienceDirect

Polymer Testing

journal homepage: www.elsevier.com/locate/polytest

An interactive Bayesian optimization framework for intelligent design of HAMA/GelMA hybrid hydrogels

Bincan Deng [a,b], Fernando López Lasaosa [a], Dingding Chen [a,b], Caimiao Zheng [c], Yiyan He [a,*], Chen Xuan [b], Yuwen Cui [a,**], Manuel Doblaré [a,d,***]

[a] Sino-Spain Joint Laboratory on Biomedical Materials (S2LBM), College of Materials Science and Engineering, Nanjing Tech University, Nanjing, 211899, China
[b] School of Mathematics and Physics, Xi'an Jiaotong-Liverpool University, Suzhou, 215123, China
[c] Department of Civil Engineering, Design School, Xi'an Jiaotong-Liverpool University, Suzhou, 215123, China
[d] Tissue Microenvironment Lab, Aragón Institute of Engineering Research (I3A), Universidad de Zaragoza, Zaragoza, 50018, Spain

ARTICLE INFO

Keywords:
Hybrid hydrogels
Interactive Bayesian optimization
Rheological properties
Intelligent design

ABSTRACT

- Hyaluronic acid methacrylate (HAMA)/gelatin methacrylate (GelMA) hybrid hydrogels are extensively utilized in biomanufacturing and tissue engineering, where their rheological properties are determinants of bioprintability and functional performance. However, optimizing these behaviors remains challenging due to the complex nonlinearity and high-dimensional design space defined by hydrogel concentration and temperature. Compared with previous machine-learning studies on hydrogel systems that primarily perform forward prediction of rheological or mechanical properties, here we introduce an interactive Bayesian optimization (IBO) framework that integrates Bayesian optimization with both an environment model and a discriminative model to optimize concentration–temperature values to achieve a target viscosity. The multilayer perceptron–based environment model here proposed exhibits high predictive performance ($R^2 \geq 0.994$, RMSE = 4.68), while the support vector machine–based discriminator achieved F1 > 0.95 and AUC >0.998 in distinguishing thermosensitive regions. Through feedback-driven iterations, IBO improved efficiency and robustness in targeting viscosity, with its mean value converging from 66.01 ± 8.76 Pa s to 51.81 ± 4.38 Pa s across three rounds, reaching a qualified rate of 80%. Even under a constrained HAMA content of 0.40% (w/v), IBO generated near-target viscosities (47.64–49.64 Pa s). These results collectively demonstrate that IBO can efficiently navigate complex, nonlinear rheological landscapes and reliably converge toward user-defined performance targets with low experimental data cost, while maintaining robustness under practical formulation constraints, thereby enabling efficient and directed formulation design. Overall, IBO provides an efficient, reliable, and scalable paradigm for viscosity-guided formulation design of HAMA/GelMA hybrid hydrogels, with potential applicability to soft matter and polymer systems. These findings can further assist in developing hydrogel formulations with improved printability and performance in biomanufacturing and related biomedical applications.

Nomenclature	Description
BO	Bayesian optimization
EI	Expected Improvement acquisition function
GP	Gaussian process
IBO	Interactive Bayesian optimization
MLP	Multilayer perceptron
RMSE	Root mean square error
MAE	Mean absolute error
SVM	Support vector machine
HAMA	Hyaluronic acid methacrylate
GelMA	Gelatin methacrylate
OFV	Objective function value

(*continued on next column*)

(*continued*)

(*continued on next page*)

* Corresponding author.
** Corresponding author.
*** Corresponding author. Sino-Spain Joint Laboratory on Biomedical Materials (S2LBM), College of Materials Science and Engineering, Nanjing Tech University, Nanjing, 211899, China.
E-mail addresses: yiyanhe@njtech.edu.cn (Y. He), ycui@njtech.edu.cn (Y. Cui), mdoblare@unizar.es (M. Doblaré).

https://doi.org/10.1016/j.polymertesting.2026.109132
Received 29 September 2025; Received in revised form 22 January 2026; Accepted 24 February 2026
Available online 25 February 2026

(*continued*)

Nomenclature	Description
y	True viscosity value
$\hat{y}$	Predicted viscosity value
λ	Penalty coefficient in the objective function
μ	Mean value of recommended parameters (used for convergence criteria)
Xp	Preferred parameter
Xr	Recommended parameter
V_p	Viscosity of the environmental model feedback
V_t	Target viscosity
y_i	True value of sample i
$\hat{y}_i$	Predicted value of sample i

1. Introduction

The design of photo-crosslinkable hydrogels in the fields of biomanufacturing and tissue engineering must balance other important properties such as biocompatibility, structural fidelity, and programmable mechanics [1]. Hyaluronic acid methacrylate (HAMA)/gelatin methacrylate (GelMA) hybrid hydrogels represent a frontier platform in smart biomaterials development due to their programmable rheological properties and biological functions. They form three-dimensional networks via photo-initiated radical polymerization, while their rheological properties (e.g., viscosity, elastic and shear moduli) and biological functions (e.g., biocompatibility) can be dynamically tuned through the concentration, temperature, and photocrosslinking parameters [2–4].

However, the complex multi-parameter coupling between rheological properties and manufacturing parameters renders conventional "trial-and-error" design inefficient. The rheological properties (e.g., storage modulus, yield stress, and viscosity) of HAMA exhibit a concentration-dependent non-monotonic trend. Specifically, these properties increase with increasing HAMA concentration within the low-to-medium range (≤0.75% w/w), while a further increase in HAMA content (>1% w/w) leads to a decrease in the aforementioned properties. Minor changes in HAMA concentration at low levels (0.4–0.75% w/w) can induce significant viscosity variations [5,6]. GelMA undergoes temperature-dependent sol–gel transitions, with its storage modulus (G′) showing continuous changes within the transition temperature range [7]. Temperature modulates the viscosity through a synergistic mechanism: for HAMA, it accelerates the relaxation of physically entangled polymer chains; for GelMA, it promotes the partial dissociation of thermoreversible triple-helix crosslinks (driven by hydrogen bonds and hydrophobic interactions), resulting in a pronounced viscosity decrease and highly nonlinear rheological behavior [8,9]. Furthermore, the synergistic interplay among photocrosslinking intensity, concentration, and temperature creates a vast parameter space. This complexity demands exhaustive rheological characterization, making experimental screening prohibitively costly and limiting application-specific performance design.

Artificial intelligence (AI) offers a new paradigm to address these challenges [10,11]. In previous hydrogel research, machine learning approaches have mainly focused on predicting rheological or mechanical properties [12,13]. For example, Deng et al. proposed Hydro-ThermoMLP for viscosity prediction, achieving an R^2 of 0.9796 under shear-thinning conditions [14]. However, these models typically function as static regressors and lack the ability to actively guide experimental selection or accommodate compositional and thermal constraints. Among available AI techniques, Bayesian optimization (BO) has gained attention due to its sample efficiency and global search capability [15,16]. In materials engineering, BO employs surrogate models (e.g., Gaussian processes) to quantify parameter–performance relationships and uses acquisition functions to identify the most informative experimental points, theoretically reducing optimization iterations by more than 60% [17]. Some previous studies have applied BO to polymer synthesis, structure–property mapping [18], high-entropy alloys, and 2D materials discovery [19–21], accelerating experimentation and uncovering non-intuitive formulations. However, despite these advances, the utilization of BO in hydrogel formulation design remains largely unexplored.

Nevertheless, the applicability of conventional BO frameworks to photocrosslinkable hydrogel systems is hindered by two critical bottlenecks. First, the strongly non-convex rheological behavior of HAMA–GelMA across the parametric space is not captured by Gaussian process kernels with stationarity assumptions, causing the optimization to easily become trapped in local optima [9,22]. Second, biomanufacturing scenarios often require achieving target properties (e.g., viscosity) under hard constraints (e.g., printing temperature, component concentrations). Conventional BO typically addresses constraints through penalty-based strategies that rely on empirical adjustment; however, excessive constraints substantially increase marginal validation costs and require repetitive experiments across different design strategies, ultimately undermining the sample efficiency advantage of BO [23,24].

To address these challenges, this study proposes an interactive Bayesian optimization (IBO) framework for viscosity optimization of HAMA/GelMA hydrogels. Our interactive IBO framework integrates two key auxiliary models to advance traditional BO: a multilayer perceptron (MLP)-based environment model [25] that enforces physical constraints for high-accuracy prediction (e.g., of non-negative viscosity) and stabilizes convergence; and a support vector machine (SVM)-based discriminator model [26], that distinguishes thermosensitive from non-thermosensitive regions to effectively mitigate systematic errors from thermal transitions. Furthermore, IBO adopts a feedback–iteration mechanism that dynamically updates both models as experimental data accumulate, progressively steering the optimization toward the target viscosity range of 50 Pa s ± 10%. By the third iteration, IBO achieved an 80% experimental success rate. Importantly, IBO maintained optimization performance under design restrictions such as HAMA concentration limits, generating application-specific formulations that satisfy target requirements. As a result, this study provides an efficient, robust, and constraint-compatible pathway for intelligent hydrogel design based on rheological properties.

The layout of this paper is as follows. Section 2 introduces the dataset and the proposed IBO framework. Section 3 presents the experimental results and their analysis. Section 4 discusses the limitations of the current study and outlines directions for future work. Finally, Section 5 concludes the paper with a summary of the main findings.

2. Methodology

This study introduces an IBO framework that integrates three core components: Bayesian optimization, an environment model, and a discriminator model. The BO module efficiently explores the parametric space to identify the most likely candidate solutions to achieve the target viscosity. The environment model serves as a data-driven surrogate for the experimental system, enabling rapid viscosity prediction under given parameter conditions. The discriminator model further evaluates these recommendations, specifically identifying whether they fall within the thermosensitive region to guarantee their validity. Through iterative interaction among these components, the IBO framework enables adaptive prediction optimization, systematic parameter recommendation, and continuous model refinement guided by experimental feedback. To improve clarity of the methodology, a concise workflow summary is presented below: (i) viscosity data from multiple HAMA/GelMA formulations are collected and preprocessed; (ii) the MLP-based environment model is trained to approximate the viscosity-parameter relationship; (iii) the SVM discriminator is constructed to classify thermosensitive versus non-thermosensitive regions; and (iv) BO iteratively proposes new experimental conditions, which are then tested and fed back to update both models.

2.1. Dataset

The initial dataset was constructed from viscosity measurements of various HAMA/GelMA hybrid hydrogel formulations using a Discovery Hybrid Rheometer (DHR-1, TA Instruments, USA) (refer to Supplementary Table S1 and S2, and Preparation of HAMA and GelMA for material sources, experimental instruments and synthesis protocols). In total, 15 distinct formulations were prepared and measured across ramp temperatures at a constant shear rate of 1 s^{-1} (Table 1). Following data cleaning and outlier handling, where viscosity-temperature curves were examined to ensure physically consistent trends, the dataset comprised 17,537 viscosity data points, which served as the foundation for the first iteration. All processed data have been stored in the project database DIAMOOC [27].

2.2. Bayesian optimization

In this study, Bayesian optimization (BO) employs a Gaussian process [28] as the surrogate model and utilizes the Expected Improvement (EI) acquisition function for parameter recommendation (chosen for its stable exploration–exploitation balance and robustness under limited samples). Specifically, BO receives variable inputs from the experimental environment, including bioink concentration and temperature, along with their corresponding viscosity measurements. Through the interplay of the surrogate model and the acquisition function, BO is able to recommend experimental parameters (HAMA concentration, GelMA concentration, and temperature) that meet the target viscosity. Moreover, by incorporating a penalty term into the objective function value (OFV), the framework enables optimization under directional and constrained conditions (Eq. (1)). The parameter space used in BO is summarized in Table 2.

$$\mathrm{OFV} = |V_P - V_t| + \lambda \cdot |X_r - X_p|, \tag{1}$$

where, V_p denotes the viscosity of the environmental model feedback, V_t represents the target viscosity (it was set at 50 Pa s in this study), X_r is the recommendation parameter (HAMA concentration, GelMA concentration, or temperature), and X_p indicates the preferred parameter. The coefficient λ serves as the penalty weight for temperature deviation and was optimized to 0.8 through a small-scale grid search ($\lambda \in \{0.1, 0.2, 0.3, 0.4, 0.5, 0.6, 0.8, 0.9, 1.0\}$), as this value provided the most stable convergence without over-penalizing temperature variations.

2.3. Environment model

Within the IBO framework, a MLP is employed as the environment model to predict viscosity under given concentration and temperature inputs [29]. The HAMA/GelMA dataset is split into training and test sets at a 7:3 ratio for hyperparameter tuning and performance evaluation. Based on the optimized hyperparameters (refer to Supplementary Table S3), the model is retrained on the full dataset to obtain the final environment model. Considering the unilateral distribution characteristic (viscosity $\geq$0 Pa s), a ReLU-based constraint term is incorporated into the loss function design [30]:

$$\mathrm{Loss} = \frac{1}{N}\sum_{i=1}^{N}(y_i - \hat{y}_i)^2 + \lambda \frac{1}{N}\sum_{i=1}^{N}\max(0, -\hat{y}_i), \tag{2}$$

where N is the total number of data samples, y_i represents the true value of the i-th sample, $\hat{y}_i$ denotes the predicted value, and λ denotes the constraint term coefficient (optimized to 0.3 through grid search). This design effectively constrains the model's output space by penalizing negative predictions, thereby enforcing compliance with the target domain's physical constraints (viscosity non-negativity).

Table 1
Formulations and measurement parameters of HAMA/GelMA Hydrogels in the experimental design for the initial dataset.

Measurements	Formulations (HAMA/GelMA)	Measurement parameters
Viscosity Vs Ramp Temperature	0.4 : 4.0% (w/v) 0.4 : 4.5% (w/v) 0.4 : 5.0% (w/v) 0.4 : 5.5% (w/v) 0.4 : 6.0% (w/v) 0.7 : 4.0% (w/v) 0.7 : 4.5% (w/v) 0.7 : 5.0% (w/v) 0.7 : 5.5% (w/v) 0.7 : 6.0% (w/v) 1.0 : 4.0% (w/v) 1.0 : 4.5% (w/v) 1.0 : 5.0% (w/v) 1.0 : 5.5% (w/v) 1.0 : 6.0% (w/v)	Diameter: 40 mm Gap: 250 μm Loading Gap: 45000 μm Room Temperature: 20 °C Temperature Range: 0-40 °C Soak Time: 30 s Measure Points: 40 Ramp rate: 2°/min Shear rate: 1 s^{-1}

Table 2
Parameter space of HAMA Concentration, GelMA Concentration, and Temperature for Bayesian optimization.

	Range	Remark
HAMA (% w/v)	0.4-1.0	Continuous parameter space
GelMA (% w/v)	4.0-6.0	
Temperature (°C)	1.0-40.0	

2.4. Discriminative model

With the introduction of thermosensitive GelMA, HAMA/GelMA formulations exhibit pronounced thermo-responsive behavior within specific temperature ranges where viscosity decreases sharply with increasing temperature [31]. Consequently, recommendations that fall within this thermosensitive region are often associated with higher systematic errors. To mitigate this issue, the system was divided into thermosensitive and non-thermosensitive regions using a threshold-based classification strategy informed by gradient and continuity criteria. As shown in Fig. 1a, the viscosity of a representative formulation initially decreases slowly with temperature before undergoing a pronounced sharp drop. The gradient at each point was computed using a central-difference approximation, and candidate thresholds within the range of 1 to 10 were systematically evaluated. A threshold of 5 was selected based on visualization and separability across the dataset, and a continuity requirement of at least 15 consecutive points above the threshold was imposed to reduce noise-induced misclassification. The resulting partitioning is illustrated in Fig. 1b, where thermosensitive regions are consistently and objectively identified. Although this approach produces robust labels for the present system, the threshold selection remains partly empirical, and developing more automated or data-driven criteria represents an important avenue for future refinement. Furthermore, a discriminative model was constructed using an SVM with a radial basis function (RBF) kernel [32], taking HAMA concentration, GelMA concentration, and temperature as inputs. The SVM-based discriminative model was trained and evaluated using the same 7:3 training-test split as the environment model, and all classification metrics were computed on the test set. This model effectively identifies whether experimental conditions fall within the thermosensitive region, thereby guiding the IBO framework and enhancing the robustness and reliability of parameter recommendations.

2.5. Interactive Bayesian optimization

Fig. 2 illustrates the cooperative roles of BO, the environment model, and the discriminative model within the IBO framework. Together, these components generate recommendations for HAMA concentration, GelMA concentration, and temperature (hereafter referred to

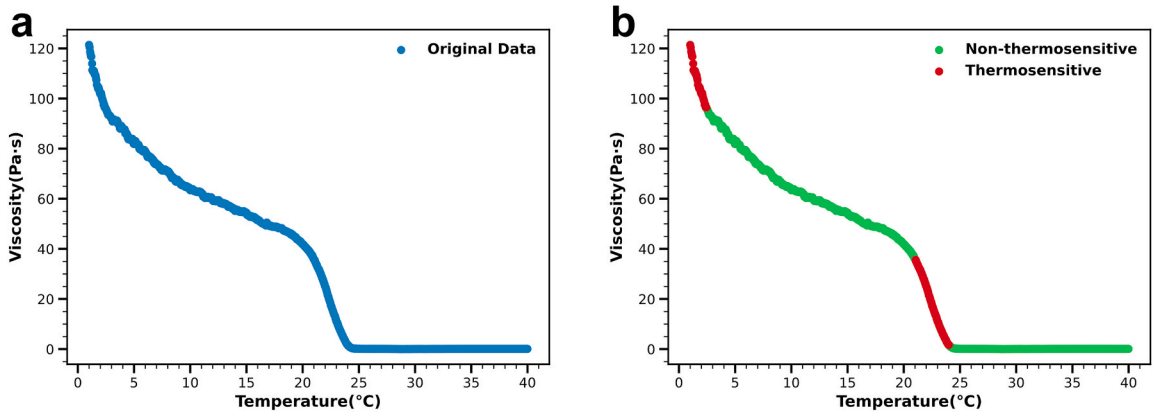

Fig. 1. An example of the viscosity-temperature relationship (a) and corresponding thermosensitive partitioning (b).

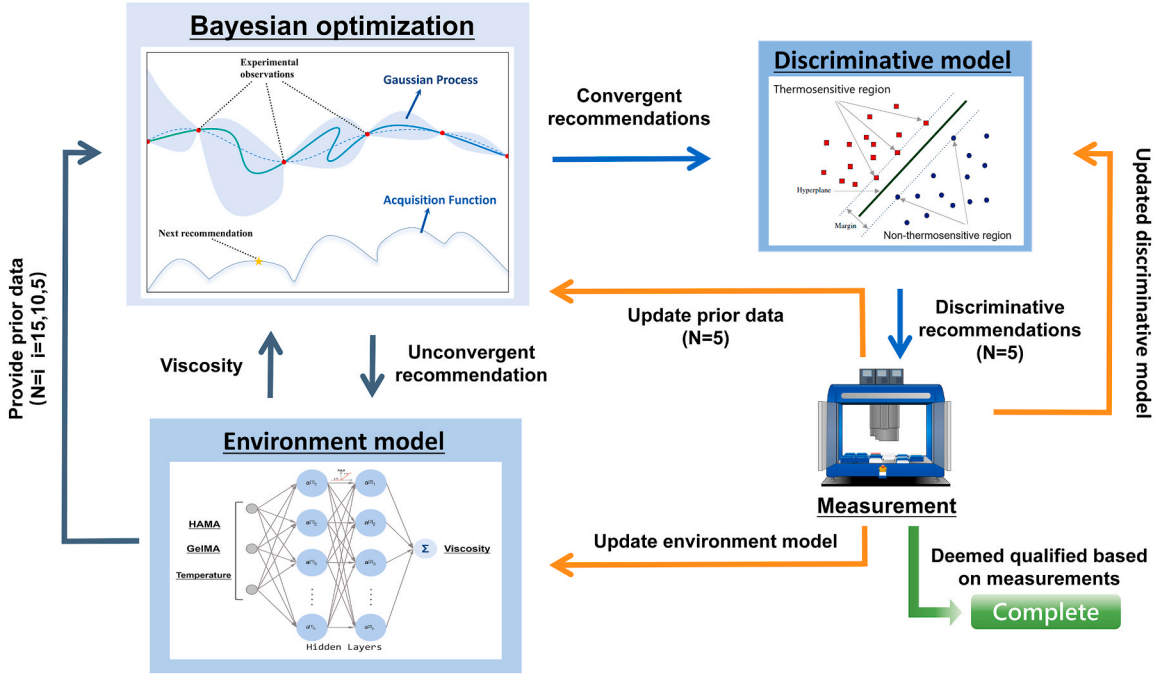

Fig. 2. Schematic diagram of the interactive Bayesian optimization (IBO) framework, illustrating the information flow among the BO module, the MLP-based environment model, and the SVM discriminative model.

collectively as "recommendations") toward the target viscosity of 50 Pa s. The recommendations are subsequently validated by rheological experiments, which accept a measurement error tolerance of 10%; recommendations within this margin are deemed qualified (i.e., viscosity measurements within 50 Pa s ±10% are considered acceptable). The resulting experimental outcomes are then used to iteratively update the models.

In the first iteration, the environment model randomly generates 15 prior datasets for BO. Specifically, these random samples are generated by sampling points in the parameter space, for which the MLP-based environment model then predicts the viscosity. This approach minimizes the potential uncontrollable noise introduced by random sampling from the existing training set, as the MLP's predictions are based on the overall data distribution, providing a more controlled prediction noise level. Subsequently, the BO model generates recommendations and sends them back to the environment model for prediction. The predicted results are subsequently fed back to BO, guiding the next round of recommendations. Convergence is determined once ten consecutive recommendations show minimal variation, which is defined as remaining within μ ± 0.1% (w/v) for HAMA, μ ± 0.2% (w/v) for GelMA, and μ ± 0.5 °C for temperature, respectively, and the predicted viscosity remains stable within 50 ± 0.5 Pa s, where μ is the mean of the last ten recommendations for each respective variable, as illustrated in Fig. 3. These parameter-specific tolerances were chosen based on the practical resolution and sensitivity of the experimental system: variations of 0.1% (w/v) in HAMA fall below the formulation preparation resolution; a slightly larger tolerance of 0.2% (w/v) is appropriate for GelMA due to its broader effective concentration range; and the ±0.5 °C threshold reflects the rheometer's thermal resolution, with statistical analysis indicating that such temperature fluctuations yield an average viscosity change of only ±0.86 Pa s around the 50 Pa s region (based on three-point sampling analysis), indicating that such fluctuations do not essentially affect the optimization outcome and also help avoid convergence inside thermosensitive regions. Similarly, the viscosity convergence band of 50 ± 0.5 Pa s corresponds to approximately 1% variation, well below the approximately 10% experimental uncertainty, ensuring that the stability criterion is stricter than measurement noise. In practice, a slightly broader tolerance (e.g., μ ± 0.2% [w/v] for

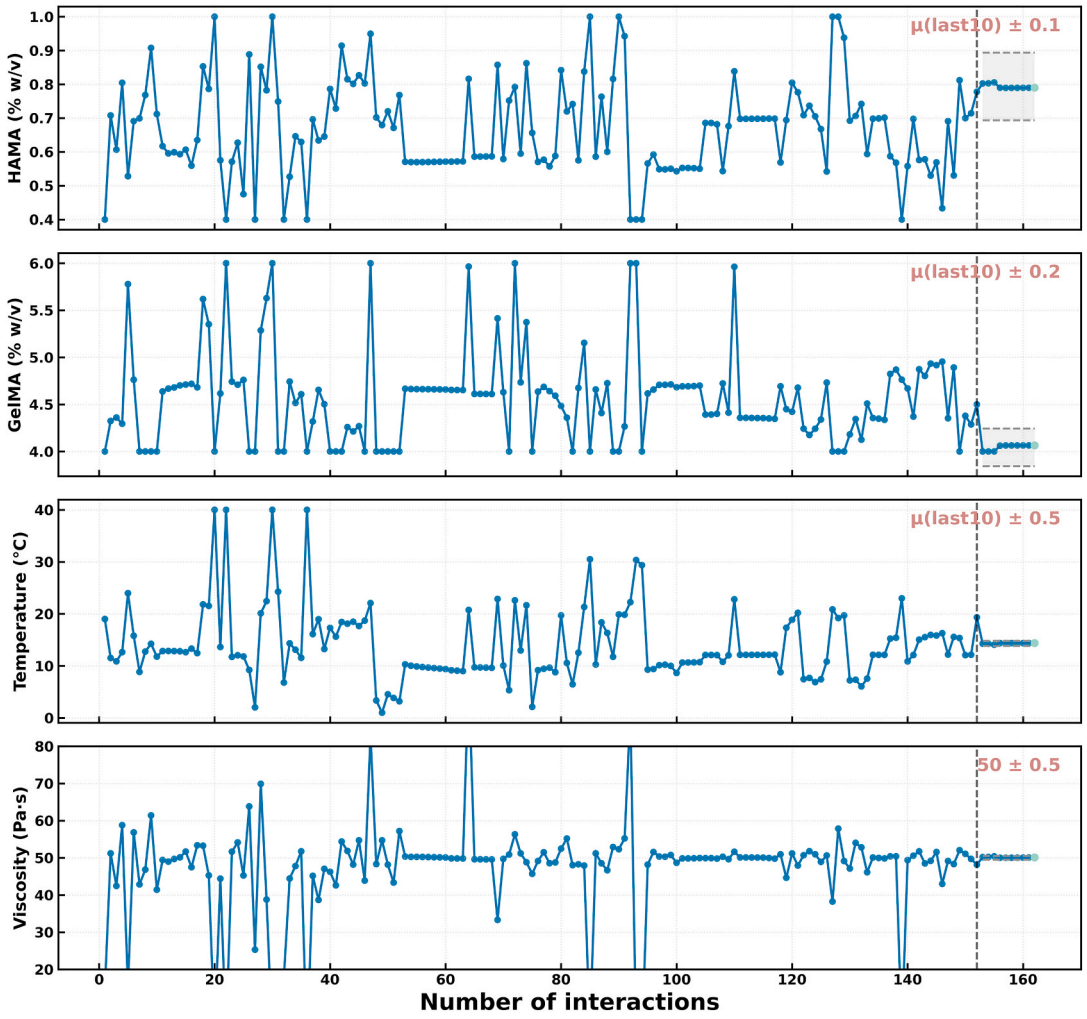

Fig. 3. An example of the convergence criteria in the IBO framework.

GelMA) was adopted to balance convergence efficiency with the intrinsic variability of the formulation process. Finally, the converged recommendations are evaluated by the discriminative model. If identified as belonging to the non-thermosensitive region, the converged recommendations are retained as final outcomes and subsequently subjected to experimental validation.

Each iteration produces five final recommendations, which are experimentally validated. The validation data are then merged with the initial dataset to form an updated dataset for retraining both the environment and discriminative models. At the same time, these five validated recommendations replace five prior samples. Consequently, in the second iteration, the prior dataset consists of the five validated recommendations from the first iteration together with ten additional randomly provided samples from the environment model, which then serve as the input for the next iteration.

To further demonstrate the capability of IBO in directed material performance design, an experimental scenario under cost constraints was introduced. Specifically, the target HAMA ratio was fixed at 0.4% (w/v) in order to reduce HAMA consumption, while maintaining the requirement that the recommended parameters achieve a viscosity of 50 Pa s under this constraint. In the second and third iterations, the first of the five final recommendations generated in each round was selected as the test case for evaluating directed performance design capability. Such constrained optimization also mirrors practical bioprinting scenarios in which formulation choices are limited by factors such as rapid crosslinking requirements, photoinitiator restrictions, and cell-viability considerations, making the ability to reach target viscosity within a restricted design space particularly valuable.

3. Results

3.1. Data distribution characteristics and variable correlation analysis

Within the IBO framework, the continuous accumulation of experimental data provides a solid foundation for optimization. As iterations progressed, the dataset expanded to 17,537, 23,383, and 28,060 entries, respectively (Fig. 4), thereby enlarging the training sample space for the models. The viscosity distribution shows that most samples fall from 0 Pa s to 200 Pa s, while fewer samples occur at the high-viscosity end (>300 Pa s), resulting in a typical long-tail distribution. This indicates that viscosity is generally moderate to low over a wide range, with only extreme conditions producing higher viscosities, thus offering exploration potential for Bayesian optimization.

Pearson correlation analysis (Fig. 5) further highlights the dominant factors within the system. GelMA concentration exhibits a strong positive correlation with viscosity, with the correlation coefficient gradually decreasing from $r = 0.40$ to $r = 0.36$ across iterations, suggesting that this effect remains robust despite repeated sampling. In contrast, temperature shows a strong negative correlation with viscosity, with the coefficient decreasing from $r = -0.71$ to $r = -0.74$, consistent with the rheological behavior of thermosensitive hydrogels, where network relaxation and reduced hydration upon heating cause a rapid viscosity

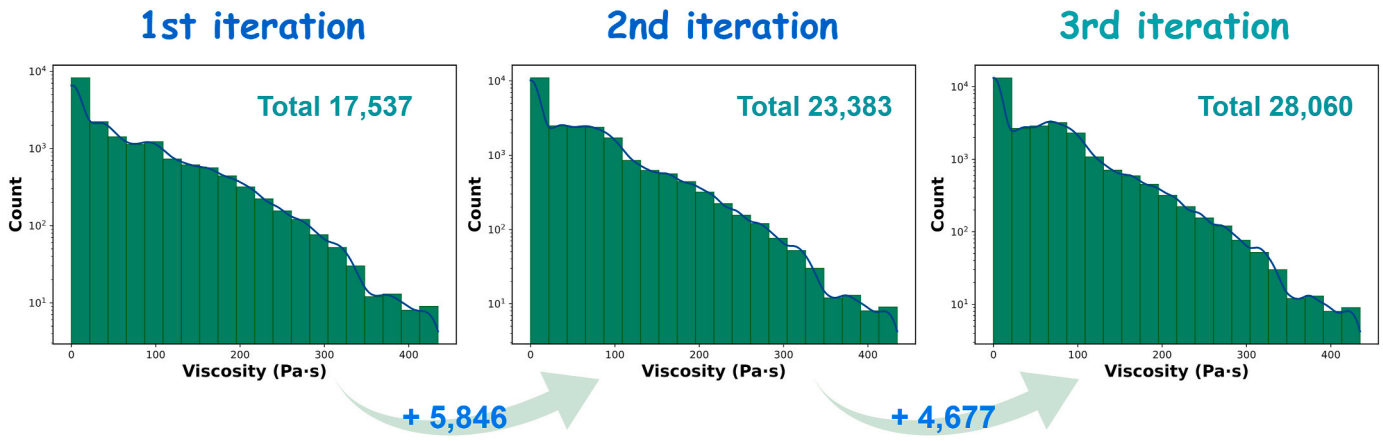

Fig. 4. Data entries and their distribution across three iterations.

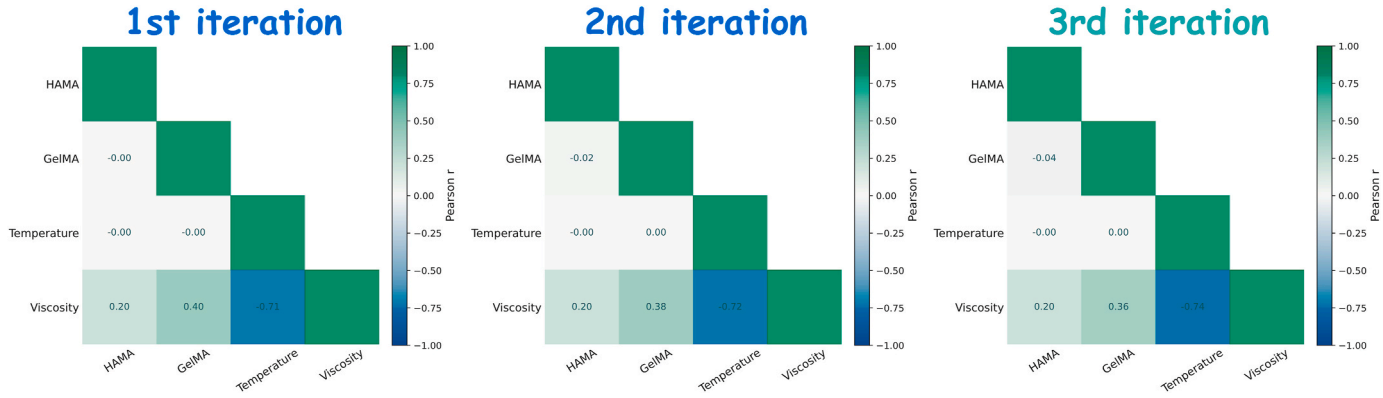

Fig. 5. Pearson correlation analysis of the dataset across three iterations.

drop [33]. HAMA concentration exhibits only a weak positive linear correlation with viscosity (r = 0.20), which should be interpreted in the context of its substantially lower concentration range compared with GelMA within the explored formulation space. As a result, variations in HAMA contribute less to the overall variance in viscosity when assessed using linear correlation metrics, and therefore do not emerge as a primary viscosity-driving factor at the global scale. Consistent with this interpretation, nonparametric correlation analysis further demonstrates a statistically significant yet temperature-dependent monotonic relationship between HAMA concentration and viscosity, with Kendall's τ (Supplementary Table S4) indicating moderate monotonicity in the intermediate temperature range (25 to 37 °C) and weaker monotonicity at lower and higher temperatures, confirming that the HAMA effect is nonlinear and conditional rather than uniformly linear across the formulation space. It is crucial to note that the limited linear correlation does not diminish the functional significance of HAMA. Rather than solely influencing viscosity, HAMA acts predominantly as a structural and regulatory component that stabilizes the network architecture and enhances formulation robustness, thereby modulating the overall physicochemical behavior of the hydrogel system [34].

3.2. Environment model

The environment model based on the MLP showed progressively improved predictive performance over three iterations. In the first iteration, the model achieved an R^2 of 0.994 and an RMSE of 5.68 on the test set (Fig. 6a), indicating overall high accuracy but with slight deviations in the medium-to-high viscosity range. In the second iteration, R^2 increased to 0.995 and RMSE decreased to 4.83 (Fig. 6b), demonstrating enhanced generalization at higher viscosities as the dataset expanded. By the third iteration, the model further converged with $R^2 = 0.994$ and RMSE = 4.68 (Fig. 6c). Furthermore, the MAE converged from 3.53 to 2.78, reflecting a stable predictive ability. These results confirm that the IBO framework can iteratively refine the environment model through feedback learning, ultimately achieving high precision in viscosity prediction which yet supports reliable parameter recommendation.

3.3. Discriminative model

The discriminative model exhibited high stability across all three iterations, effectively distinguishing between thermosensitive and non-thermosensitive regions. Using the SVM with an RBF kernel, the model achieved F1 scores of 0.980, 0.970, and 0.964 in the first, second, and third iterations, respectively (Fig. 7a–c), all remaining above 0.95. The slight decrease in F1 score was mainly due to class imbalance and dataset shifts introduced during supplementation, rather than degradation of model performance (Fig. 7d). Meanwhile, the Area Under the Curve (AUC) consistently exceeded 0.998 in all iterations, further confirming the robustness of the model across different dataset sizes and its ability to mitigate systematic errors arising from thermosensitive conditions. The confusion matrix shows that the model performed exceptionally well in identifying non-thermosensitive samples, with both false positive and false negative rates remaining very low. This indicates that the model not only captured the boundary features of the thermosensitive region with high precision but also maintained consistency under large-scale experimental conditions. Collectively, the inclusion of the discriminative model before final recommendation significantly enhanced the validity of IBO outcomes and improved the success rate of experimental validation.

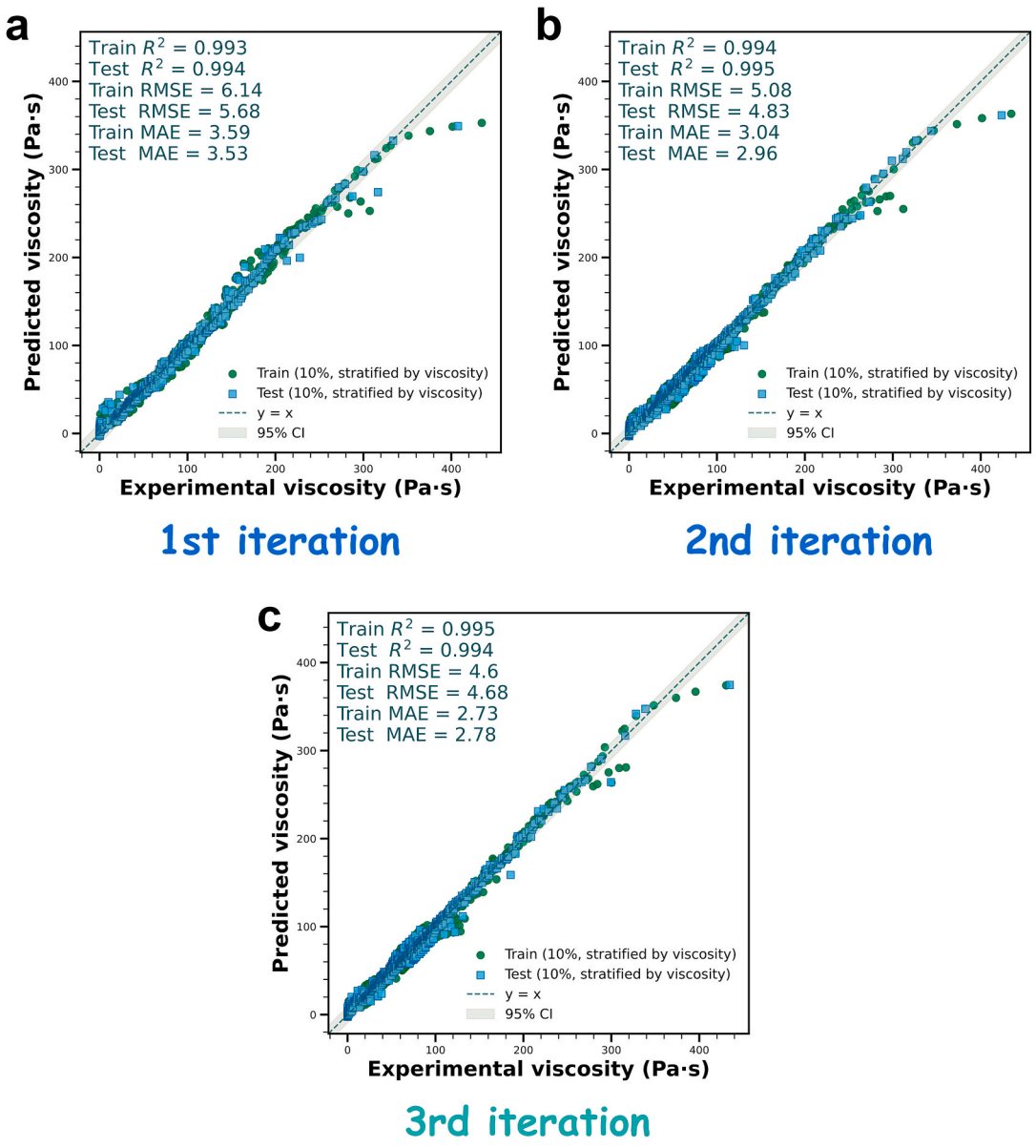

Fig. 6. Performance of the environment model across three rounds of iterations.

3.4. *Interactive Bayesian optimization*

Under the guidance of the IBO framework, five recommendations were generated in each iteration and validated through rheological experiments. In the first iteration, viscosities ranged from 54.19 to 78.60 Pa s, with only one result falling within the target range (50 Pa s ±10%), while the others were higher (Fig. 8a). In the second iteration, the results improved markedly, with three recommendations (R-1, R-3, R-5) within the target range, indicating convergence (Fig. 8b). By the third iteration, the recommendations became more stable, with four values qualified; notably, R-1 and R-5 reached 49.64 and 48.70 Pa s, respectively, in excellent agreement with the target (Fig. 8c).

To further assess convergence, the mean and standard deviation of viscosities were calculated across iterations (Fig. 8d). The first iteration yielded a mean of 66.01 ± 8.76 Pa s, substantially above the target with high variability. In the second iteration, the mean decreased to 58.04 ± 8.12 Pa s, approaching the target, while the third iteration converged further to 51.81 ± 4.38 Pa s, nearly identical to the target and with significantly reduced variance. Given that hydrogel viscosity measurements typically allow an experimental uncertainty of about 10%, the standard deviation obtained in the third iteration already fell within this acceptable range. Under such conditions, further IBO iterations (e.g., a fourth or fifth round) would be expected to yield only marginal refinements, as the achievable improvement becomes increasingly constrained by intrinsic experimental noise rather than optimization efficiency, rendering additional IBO iterations unlikely to provide physical gains. Overall, the iterative updates within the IBO framework not only steered the recommendations toward the target but also reduced experimental variability, achieving both convergence and robustness.

To further validate optimization under constraints, HAMA content was fixed to 0.40% (w/v) during the second and third iterations. Even with this constraint, IBO successfully generated recommendations near the target viscosity. Specifically, in the second iteration, the constrained R-1 formulation yielded 47.64 Pa s, meeting both the target range and the HAMA lower-limit constraint. In the third iteration, the result improved further to 49.64 Pa s, closely matching the target. These findings clearly indicate that the IBO framework enables precise viscosity optimization under both unconstrained and constrained conditions, providing a methodological advantage for the practical

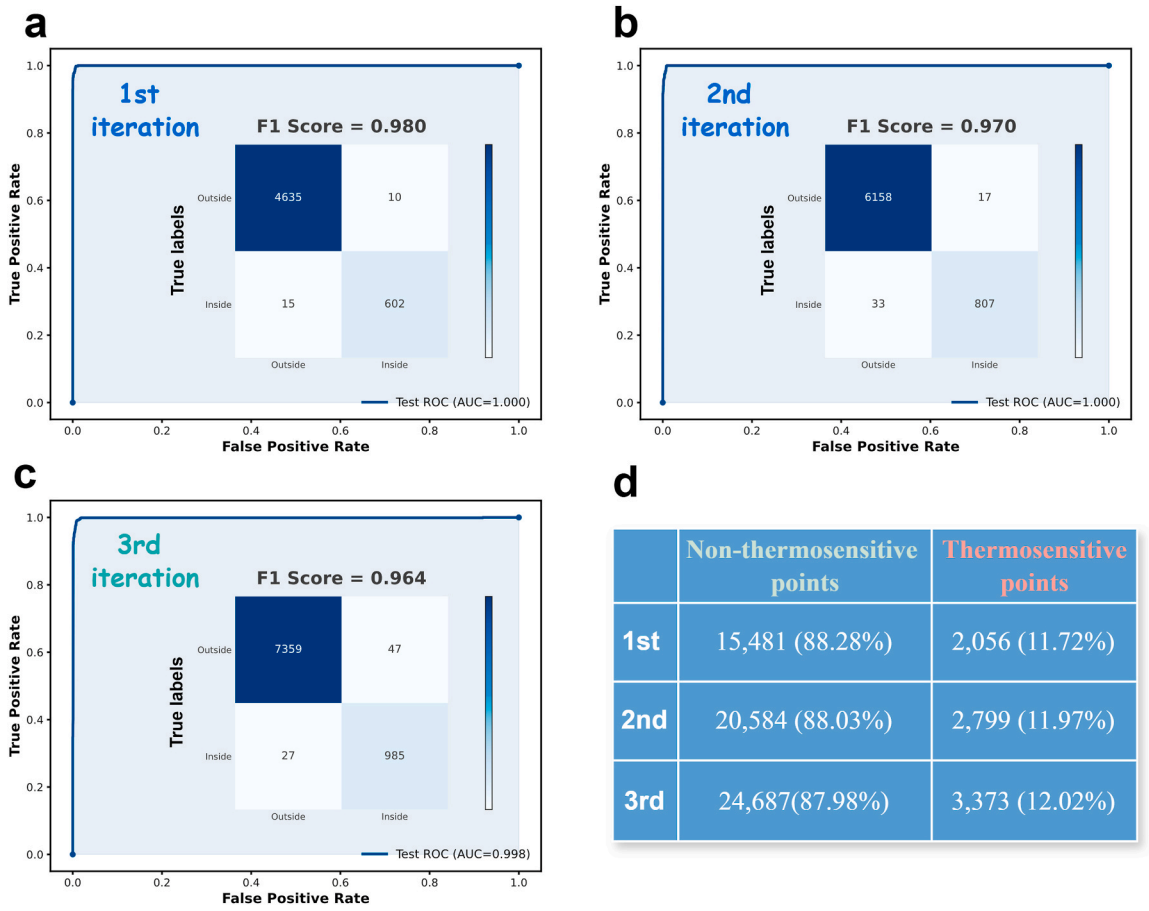

Fig. 7. Classification performance of the discriminative model across three iterations (a–c), together with the evolution of the number of classified data points (d).

application and controllable design of hydrogel systems.

To benchmark the proposed IBO framework, simulation baseline comparisons with conventional Bayesian optimization (BO) and the standard design of experiments (DoE) were conducted (refer to Supplementary Baseline comparisons). IBO achieved a markedly higher success rate (up to 80% in the third iteration, 53% overall) compared with BO (7.81%) and DoE sampling (4.35%), demonstrating substantially improved optimization efficiency under limited experimental budgets.

In brief, the IBO framework demonstrated clear advantages through data-driven feedback iterations. With successive iterations, the environment model achieved progressively higher predictive accuracy, the discriminative model maintained consistently high classification performance, and the recommendations converged steadily toward the target. Notably, analysis of mean and standard deviation showed that viscosities evolved from excessively high and variable in the first iteration to highly precise and stable in the third, confirming the effectiveness and scalability of IBO for formulation optimization. Furthermore, under the constrained scenario with fixed HAMA content, IBO continued to provide valid recommendations, highlighting its potential for multi-objective and constrained optimization tasks. Collectively, these results establish IBO as an efficient and reliable pathway for viscosity control and directed material design.

4. Discussion

This study demonstrates that the IBO framework enables efficient viscosity optimization in the binary HAMA/GelMA system. Such viscosity-directed optimization is directly relevant to bioprinting scenarios in which cell-laden constructs require bioinks that balance printability, rapid crosslinking, and cell viability, making adaptive and constraint-aware formulation design particularly valuable [35,36]. In addition, the framework integrates an accurate environment model and an effective discriminative model, allowing robust convergence toward user-defined viscosity targets even under constrained formulation conditions. Furthermore, the rheological patterns observed in this work arise from the complementary physical roles of the two components. HAMA increases viscosity through concentration-dependent chain entanglement, while GelMA exhibits thermosensitivity due to reversible triple-helix crosslinking that reduces viscosity upon heating. The combined effects of these mechanisms lead to the nonlinear concentration-temperature behavior captured by the optimization process.

However, the applicability of the proposed framework to more complex ternary or multicomponent systems remains to be validated, as stronger nonlinear couplings may compromise its efficiency and stability. Although the environment model achieved high accuracy on the test set, prediction errors affected by experimental noise occasionally produced non-physical behaviors, such as decreasing viscosity with increasing HAMA concentration. In addition, while the discriminative model effectively reduces systematic errors originating from the thermosensitive region, it currently operates largely independently of the optimization process, underscoring the need for tighter integration between the two components. Furthermore, several convergence thresholds employed in this study were empirically selected, making it difficult to directly transfer these criteria to other hydrogel systems. Crucially, the use of a single HAMA content constraint of 0.40% (w/v) does not fully reflect the IBO framework's ability to handle constraints, as it needs to account for the broader applicability of the framework under more complex, multi-parameter constraints.

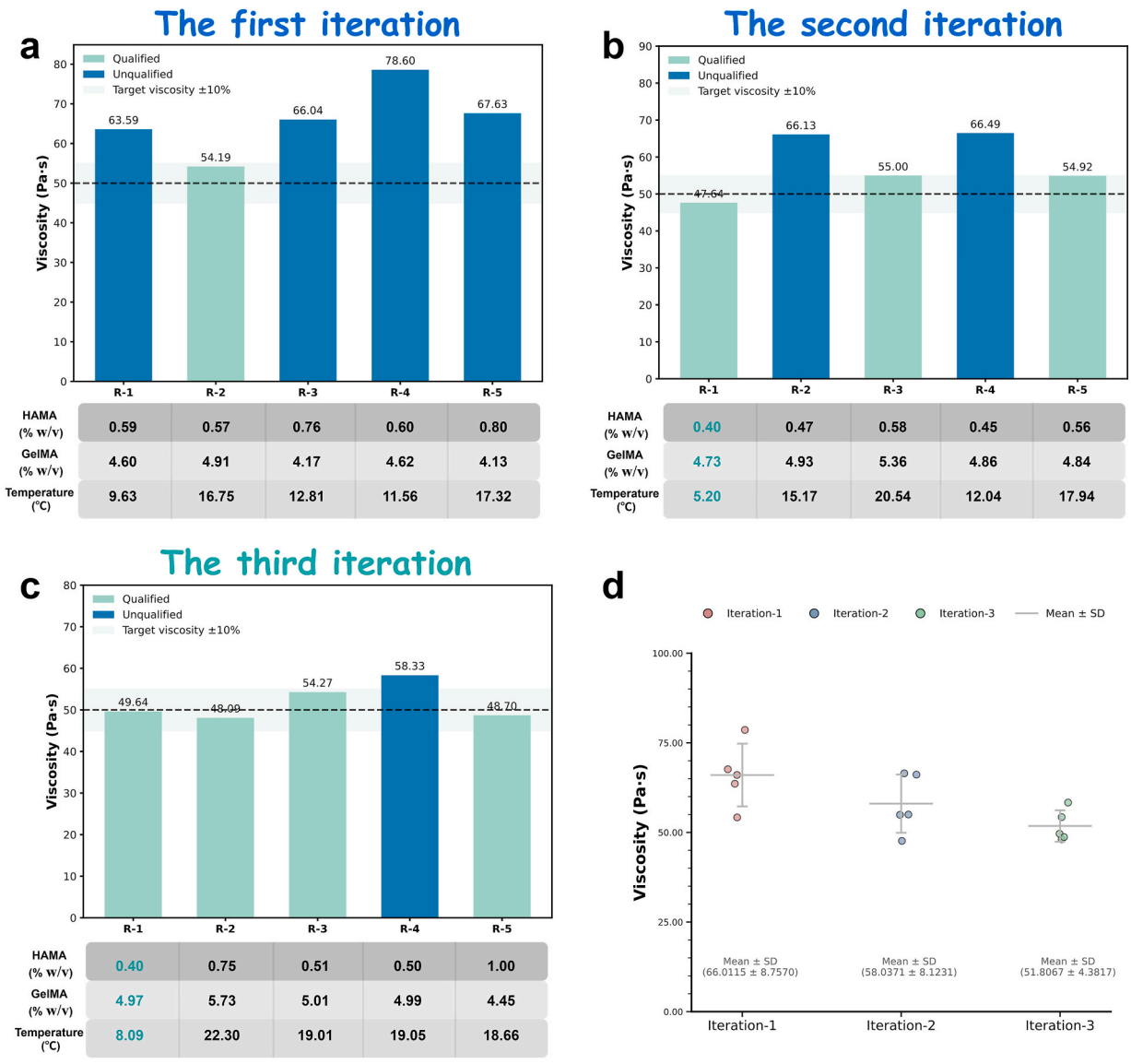

Fig. 8. Experimental validation of recommendations across three iterations.

To address occasional non-physical predictions and improve consistency with known material behavior, future work may incorporate physics-informed neural networks (PINNs) or hybrid modeling strategies [14,37], which could enforce monotonicity and other physical constraints while enabling more reliable extrapolation beyond the training domain. Additional improvements may involve developing automated or data-driven strategies for thermosensitive-region classification and coupling the discriminative model more closely with the optimization objectives. Regarding convergence-threshold selection, future studies should establish more generalizable, experimentally grounded criteria to improve the portability of the IBO framework across different material systems. Moreover, future research will focus on conducting more comprehensive experiments, including testing recommendations under multi-parameter constraints and exploring the validity of recommendations beyond the current parameter space. Overall, when combined with active learning, transfer learning, and high-throughput experimentation, the IBO framework has strong potential to accelerate directed materials design across soft matter and polymer systems [38,39].

5. Summary and conclusions

This work establishes an Interactive Bayesian Optimization (IBO) framework that integrates an environment model with a discriminative model to enable high-precision viscosity prediction and intelligent recommendation for HAMA/GelMA hybrid hydrogel systems under physical constraints. Based on the findings of this study, the following conclusions can be drawn:

1) The MLP-based environment model exhibited excellent robustness and predictive accuracy across iterations ($R^2 \geq 0.994$, RMSE reduced to 4.68), supporting continuous viscosity optimization.
2) The SVM-based discriminative model consistently achieved superior performance in identifying thermosensitive regions (F1 $>$ 0.95, AUC $>$0.998), effectively minimizing systematic errors under high-risk conditions.
3) Through iterative feedback, IBO substantially enhanced design efficiency and success rates: the mean viscosity of recommendations converged from 66.01 $\pm$ 8.76 Pa s in the first iteration to 51.81 $\pm$ 4.38 Pa s in the third, with an 80% hit rate within the target range.

4) Even under strict formulation constraints (e.g., HAMA content limited to 0.40% [w/v]), IBO generated recommendations with viscosities close to the target (47.64–49.64 Pa s), demonstrating robust capability for constrained intelligent design.

Overall, IBO provides an efficient, reliable, and scalable pathway for performance optimization and intelligent design of hydrogel systems, while offering broader methodological significance and application potential for soft matter and polymeric materials. Looking forward, the framework could be further strengthened through integration with physics-informed neural networks or high-throughput experimental platforms, which may enhance both physical fidelity and data-efficiency in future hydrogel design.

CRediT authorship contribution statement

Bincan Deng: Conceptualization, Data curation, Formal analysis, Investigation, Methodology, Software, Validation, Visualization, Writing – original draft. **Fernando López Lasaosa:** Data curation, Resources. **Dingding Chen:** Conceptualization. **Caimiao Zheng:** Visualization. **Yiyan He:** Supervision, Writing – review & editing. **Chen Xuan:** Conceptualization, Supervision, Writing – review & editing. **Yuwen Cui:** Conceptualization, Funding acquisition, Investigation, Methodology, Supervision, Writing – review & editing. **Manuel Doblaré:** Conceptualization, Supervision, Validation, Writing – review & editing.

Declaration of competing interest

The authors declare that they have no known competing financial interests or personal relationships that could have appeared to influence the work reported in this paper.

Acknowledgments

This work was supported by the National Key R&D Program of China (2022YFE0124500). Manuel Doblaré acknowledges the financial support from Beonchip S.L. through the project DIAMOOC IDI-20220819. Chen Xuan also acknowledges the National Natural Science Foundation of China (12211530416, 12002287) and the Research Development Fund of Xi'an Jiaotong-Liverpool University (RDF-22-01-011) for their funding support.

Appendix A. Supplementary data

Supplementary data to this article can be found online at https://doi.org/10.1016/j.polymertesting.2026.109132.

Data availability

The data that support the findings of this study are available in the Supplementary (Dataset.xlsx).

References

[1] Y. Wang, S. Zhang, J. Wang, Photo-crosslinkable hydrogel and its biological applications, Chin. Chem. Lett. 32 (5) (2021) 1603–1614, https://doi.org/10.1016/j.cclet.2020.11.073.

[2] E.S. Lisboa, C. Serafim, W. Santana, V.L.S. dos Santos, R.L.C. de Albuquerque-Junior, M.V. Chaud, J.C. Cardoso, S. Jain, P. Severino, E.B. Souto, Nanomaterials-combined methacrylated gelatin hydrogels (GelMA) for cardiac tissue constructs, J. Contr. Release 365 (2024) 617–639, https://doi.org/10.1016/j.jconrel.2023.11.056.

[3] P. Chansoria, S. Asif, K. Polkoff, J. Chung, J.A. Piedrahita, R.A. Shirwaiker, Characterizing the effects of synergistic thermal and photo-cross-linking during biofabrication on the structural and functional properties of gelatin methacryloyl (GelMA) hydrogels, ACS Biomater. Sci. Eng. 7 (11) (2021) 5175–5188, https://doi.org/10.1021/acsbiomaterials.1c00635.

[4] B. Velasco-Rodriguez, T. Diaz-Vidal, L.C. Rosales-Rivera, C.A. García-González, C. Alvarez-Lorenzo, A. Al-Modlej, V. Domínguez-Arca, G. Prieto, S. Barbosa, J.F. A. Soltero Martínez, P. Taboada, Hybrid methacrylated gelatin and hyaluronic acid hydrogel scaffolds. Preparation and systematic characterization for prospective tissue engineering applications, Int. J. Mol. Sci. 22 (13) (2021) 6758, https://doi.org/10.3390/ijms22136758.

[5] A. Abbadessa, M. Landín, E. Oude Blenke, W.E. Hennink, T. Vermonden, Two-component thermosensitive hydrogels: phase separation affecting rheological behavior, Eur. Polym. J. 92 (2017) 13–26, https://doi.org/10.1016/j.eurpolymj.2017.04.029.

[6] S.J. Haward, A. Jaishankar, M.S.N. Oliveira, M.A. Alves, G.H. McKinley, Extensional flow of hyaluronic acid solutions in an optimized microfluidic cross-slot device, Biomicrofluidics 7 (4) (2013), https://doi.org/10.1063/1.4816708.

[7] C.G. Gaglio, D. Baruffaldi, C.F. Pirri, L. Napione, F. Frascella, GelMA synthesis and sources comparison for 3D multimaterial bioprinting, Front. Bioeng. Biotechnol. 12 (2024), https://doi.org/10.3389/fbioe.2024.1383010.

[8] M.K. Cowman, T.A. Schmidt, P. Raghavan, A. Stecco, Viscoelastic properties of hyaluronan in physiological conditions, F1000Research 4 (2015) 622, https://doi.org/10.12688/f1000research.6885.1.

[9] A.T. Young, O.C. White, M.A. Daniele, Rheological properties of coordinated physical gelation and chemical crosslinking in gelatin methacryloyl (GelMA) hydrogels, Macromol. Biosci. 20 (12) (2020), https://doi.org/10.1002/mabi.202000183.

[10] S. Uppalapati, P. Paramasivam, N. Kilari, J.S. Chohan, P.K. Kanti, H. Vemanaboina, L.H. Dabelo, R. Gupta, Precision biochar yield forecasting employing random forest and XGBoost with taylor diagram visualization, Sci. Rep. 15 (1) (2025), https://doi.org/10.1038/s41598-025-91450-w.

[11] P. Paramasivam, P.K. Kanti, A. Dubey, D. Balasubramanian, U. Kale, A. Kilikevičius, Explainable prognostics-optimization of hydrogen carrier biogas engines in an integrated energy system using a hybrid game-theoretic approach with XGBoost and statistical methods, Int. J. Hydrogen Energy 160 (2025) 150585, https://doi.org/10.1016/j.ijhydene.2025.150585.

[12] J. Li, C. Zhang, W. Lan, W. Chen, D. Huang, Machine learning-assisted strategies to enhance the mechanical properties of PVA hydrogels, J. Mech. Behav. Biomed. Mater. 168 (2025) 107027, https://doi.org/10.1016/j.jmbbm.2025.107027.

[13] W. Hong, Q. Zhang, L. Lin, H. Zhang, X. Lei, Y. Wang, D. Zhang, Z. Jia, L. Wang, J. Pang, Y. Sun, J. Liu, Machine learning - driven polysaccharide - based hydrogels: intelligent design and precision therapeutics for oral wound repair, Adv. Funct. Mater. (2025), https://doi.org/10.1002/adfm.202525950.

[14] B. Deng, S. Chen, F.L. Lasaosa, X. Xue, C. Xuan, H. Mao, Y. Cui, Z. Gu, M. Doblare, Predicting rheological properties of HAMA/GelMA hybrid hydrogels via machine learning, J. Mech. Behav. Biomed. Mater. 168 (2025) 107005, https://doi.org/10.1016/j.jmbbm.2025.107005.

[15] X. Wang, Y. Jin, S. Schmitt, M. Olhofer, Recent advances in bayesian optimization, arXiv preprint. arXiv (2022). https://arxiv.org/abs/2206.03301.

[16] P.K. Kanti, P. Sharma, B. Koneru, P. Banerjee, K.D. Jayan, Thermophysical profile of graphene oxide and MXene hybrid nanofluids for sustainable energy applications: model prediction with a bayesian optimized neural network with K-Cross fold validation, FlatChem 39 (2023) 100501, https://doi.org/10.1016/j.flatc.2023.100501.

[17] A.E. Gongora, B. Xu, W. Perry, C. Okoye, P. Riley, K.G. Reyes, E.F. Morgan, K. A. Brown, A bayesian experimental autonomous researcher for mechanical design, Sci. Adv. 6 (15) (2020), https://doi.org/10.1126/sciadv.aaz1708.

[18] X. Wang, Y. Huang, X. Xie, Y. Liu, Z. Huo, M. Lin, H. Xin, R. Tong, Bayesian-optimization-assisted discovery of stereoselective aluminum complexes for ring-opening polymerization of racemic lactide, Nat. Commun. 14 (1) (2023), https://doi.org/10.1038/s41467-023-39405-5.

[19] G.A. Sulley, J. Raush, M.M. Montemore, J. Hamm, Accelerating high-entropy alloy discovery: efficient exploration via active learning, Scr. Mater. 249 (2024) 116180, https://doi.org/10.1016/j.scriptamat.2024.116180.

[20] Y. Xian, X. Ding, X. Jiang, Y. Zhou, J. Sun, D. Xue, T. Lookman, Unlocking the black box beyond bayesian global optimization for materials design using reinforcement learning, npj Comput. Mater. 11 (1) (2025), https://doi.org/10.1038/s41524-025-01639-w.

[21] Y. Wang, G. Li, A.H. Natarajan, S. Mukerjee, X. Jin, S. Kar, Accelerating optimal synthesis of atomically thin MoS2: a constrained bayesian optimization guided brachistochrone approach, Adv. Mater. Technol. 10 (5) (2024), https://doi.org/10.1002/admt.202401465.

[22] Y.-H. Tang, D. Zhang, G.E. Karniadakis, An atomistic fingerprint algorithm for learning Ab initio molecular force fields, J. Chem. Phys. 148 (3) (2018), https://doi.org/10.1063/1.5008630.

[23] C. Bian, Q. Liu, X. Zhang, B. Yan, X. Wang, S. Zuo, H. Liu, An efficient mixed constrained bayesian optimization for handling known and unknown constraints, Adv. Eng. Inform. 62 (2024) 102704, https://doi.org/10.1016/j.aei.2024.102704.

[24] Y. Tian, T. Li, J. Pang, Y. Zhou, D. Xue, X. Ding, T. Lookman, Materials design with target-oriented bayesian optimization, npj Comput. Mater. 11 (1) (2025), https://doi.org/10.1038/s41524-025-01704-4.

[25] G.J. Gibson, C.F.N. Cowan, On the decision regions of multilayer perceptrons, Proc. IEEE 78 (10) (1990) 1590–1594, https://doi.org/10.1109/5.58343.

[26] S. Tavara, Parallel computing of support vector machines, ACM Comput. Surv. 51 (6) (2019) 1–38, https://doi.org/10.1145/3280989.

[27] DIAMOOC database–materials Powered by AI Big Data Platform, DIAMOOC database, Chengdu, 2025. Available from: http://diamooc.matclouds.com. (Accessed 15 January 2025).

[28] S. Davoodi, H. Vo Thanh, D.A. Wood, M. Mehrad, M. Al-Shargabid, V. S. Rukavishnikov, Committee machine learning: a breakthrough in the precise prediction of CO2 storage mass and oil production volumes in unconventional

reservoirs, Geoenergy Sci. Eng. 245 (2025) 213533, https://doi.org/10.1016/j.geoen.2024.213533.
[29] H. Vo Thanh, Y. Sugai, K. Sasaki, Application of artificial neural network for predicting the performance of CO2 enhanced oil recovery and storage in residual oil zones, Sci. Rep. 10 (1) (2020), https://doi.org/10.1038/s41598-020-73931-2.
[30] B. Deng, F.L. Lasaosa, D. Chen, Y. He, C. Xuan, Y. Cui, M. Doblaré, Transfer learning-enabled viscosity prediction for HAMA/GelMA hybrid hydrogels, Mater. Today Commun. 47 (2025) 113018, https://doi.org/10.1016/j.mtcomm.2025.113018.
[31] Y. Wang, H. Yue, A. Liu, Y. Cui, Y. Hou, X. Ni, R.F. Pereira, B. Huang, C. Vyas, P. Bartolo, Dual crosslinkable bioink for direct and embedded 3D bioprinting at physiological temperature, Mater. Today 85 (2025) 1–16, https://doi.org/10.1016/j.mattod.2025.02.005.
[32] S. Davoodi, H. Vo Thanh, D.A. Wood, M. Mehrad, M. Al-Shargabi, V. S. Rukavishnikov, Machine learning insights to CO2-EOR and storage simulations through a five-spot pattern – a theoretical study, Expert Syst. Appl. 250 (2024) 123944, https://doi.org/10.1016/j.eswa.2024.123944.
[33] A.S. Hoffman, Hydrogels for biomedical applications, Adv. Drug Deliv. Rev. 64 (2012) 18–23, https://doi.org/10.1016/j.addr.2012.09.010.
[34] Carl C.L. Schuurmans, M. Mihajlovic, C. Hiemstra, K. Ito, W.E. Hennink, T. Vermonden, Hyaluronic acid and chondroitin sulfate (Meth)Acrylate-Based hydrogels for tissue engineering: synthesis, characteristics and pre-clinical evaluation, Biomaterials 268 (2021) 120602, https://doi.org/10.1016/j.biomaterials.2020.120602.
[35] J. Malda, J. Visser, F.P. Melchels, T. Jüngst, W.E. Hennink, W.J.A. Dhert, J. Groll, D.W. Hutmacher, 25th anniversary article: engineering hydrogels for biofabrication, Adv. Mater. 25 (36) (2013) 5011–5028, https://doi.org/10.1002/adma.201302042.
[36] A. Ribeiro, M.M. Blokzijl, R. Levato, C.W. Visser, M. Castilho, W.E. Hennink, T. Vermonden, J. Malda, Assessing bioink shape fidelity to aid material development in 3D bioprinting, Biofabrication 10 (1) (2017) 014102, https://doi.org/10.1088/1758-5090/aa90e2.
[37] M. Galanti, M. Janssen, I. Roghair, J.-Y. Dieulot, P. Shoeibi Omrani, J. Boon, M. van Sint Annaland, Towards surrogate modeling for adsorption processes using physics-informed neural networks, Processes 13 (9) (2025) 2824, https://doi.org/10.3390/pr13092824.
[38] Y. Kim, Y. Kim, C. Yang, K. Park, G. Gu, S. Ryu, Deep Learning Framework for Material Design Space Exploration Using Active Transfer Learning and Data Augmentation, Open Engineering Inc, May 4, 2021, https://doi.org/10.31224/osf.io/k6v4q.
[39] T. Lookman, P.V. Balachandran, D. Xue, R. Yuan, Active learning in materials science with emphasis on adaptive sampling using uncertainties for targeted design, npj Comput. Mater. 5 (1) (2019), https://doi.org/10.1038/s41524-019-0153-8.